arXiv:hep-ph/9808466v1 28 Aug 1998

MADPH-98-1076
hep-ph/9808466
August, 1998

Slepton Oscillation at $e\gamma$ Colliders

J.-J. Cao[a,c], T. Han[b], X. Zhang[a], and G.-R. Lu[c]
[a]*Institute of High Energy Physics, Academia Sinica, Beijing 100039, P. R. China*
[b]*Department of Physics, University of Wisconsin, Madison, WI 53706, USA*
[c]*Department of Physics, Henan Normal University, Xinxiang, Henan, P.R. China*

Abstract

We study the possible signature for lepton-flavor violation processes in the scalar-lepton sector of the minimal supersymmetric model at future electron-photon colliders. We find that an $e\gamma$ collider can provide a good opportunity to probe the mass differences and flavor mixing angles between the sleptons of the first generation and the other two generations for the right-handed as well as the left-handed sector. The sensitivity reach for lepton-flavor violation is comparable to that obtained at an e^+e^- and e^-e^- collider, and is significantly better than the current bound from low-energy rare processes such as $\mu \to e\gamma$.

I. INTRODUCTION

Supersymmetry (SUSY) is believed to be the most promising candidate for physics beyond the Standard Model (SM). Among many attractive features, supersymmetry can provide understanding for the mass hierarchy of the weak scale and the Planck scale. The existence of the SUSY particles (sparticles) at the weak scale can satisfactorily lead to the gauge coupling unification at a desirable scale. The electroweak symmetry breaking is triggered radiatively by the large top-quark mass. The weak-scale SUSY also necessarily leads to rich physics in the near-future collider experiments [1].

However, current supersymmetric models do not advance our knowledge of flavor physics beyond the SM, such as the fermion mass generation and quark/lepton mixings. In fact, generic SUSY models often have arbitrary flavor mixings and mass parameters in the scalar quark (squark) and scalar lepton (slepton) sectors and one would have to assume certain symmetries to prevent large flavor-changing neutral currents (FCNC) [2]. On the other hand, the flavor structure in the SUSY sector motivates us to seek for new physics, and any experimental observation on the FCNC processes beyond the SM would undoubtedly shed light on our understanding for flavor physics. The evidence of neutrino oscillations observed by the Super-Kamiokande experiments serves as a good example [3].

Besides the conventional studies for FCNC effects in SUSY grand unification models in processes $b \to s\gamma$ [4], neutral meson oscillations [5], and $\mu \to e\gamma$ [6] at low energies, it has been actively pursued to explore the possible signatures at future collider experiments for the lepton-flavor violating processes in SUSY theories. Due to the super-GIM mechanism, it has been pointed out [7,8] that for low-energy rare processes induced by sparticle loops, the rates are suppressed by $\Delta M/M$; while for the flavor changing signal from direct slepton production at high energy colliders the suppression factor is at most $\Delta M/\Gamma$, where M and Γ are the sfermion mass and decay width. It is found that there is great physics potential for the CERN Large Hadron Collider (LHC) and the Next e^+e^- Linear Collider (NLC) to probe SUSY flavor physics through slepton oscillations [7,8]. In contrast, there are several advantages for considering an $e\gamma$ collider to study SUSY flavor physics. First of all, lepton and electron-photon colliders often provide much cleaner experimental environment for new physics searches than hadron colliders. Second, in models with soft mass unification or with (minimal) gauge-mediation of SUSY breaking, the lightest neutralino ($\tilde{\chi}_1^0$) is expected to be lighter than sleptons ($\tilde{\ell}$). Therefore, the sparticle production for $e^\pm\gamma \to \tilde{\ell}\tilde{\chi}^0,\ \tilde{\nu}\tilde{\chi}^\pm$ would have lower mass threshold [9–11] than those for $e^+e^- \to \tilde{\ell}^-\tilde{\ell}^+, \tilde{\nu}\tilde{\nu}^*$. Third, even when slepton pair production is kinematically allowed there is a P-wave (β^3) suppression of the cross section near threshold, and the event rates are correspondingly limited. On the other hand, the cross sections for $\tilde{\ell}\tilde{\chi}^0,\ \tilde{\nu}\tilde{\chi}^\pm$ production are proportional to β near threshold, so high production rates are achievable. Fourth, since there exists the net electron flavor in the initial state, the observation on a lepton flavor other than an electron in the final state could be a clear signature for the flavor oscillation, with less severe SM backgrounds.

In this paper, we study the signals for slepton oscillation between the first generation and the other two generations at an $e\gamma$ collider and their SM backgrounds. We consider an e^+e^- collider with 500 GeV c. m. energy and an annual luminosity 50 fb^{-1} [12], running at the $e\gamma$ mode [13]. In section II, we first illustrate the general flavor mixing in the slepton sector for the minimal supersymmetric standard model (MSSM). We then present the slepton production mechanisms and cross sections with and without the flavor mixing. In section III, we study the slepton oscillation signals and their SM backgrounds at an $e\gamma$ collider. We find that for the gaugino-like neutralino and chargino, it is promising to probe the mass differences and mixing angles between the left-handed sleptons to good precision. For the right-handed slepton sector, the results are comparable to the existing one at e^+e^- and e^-e^- linear colliders [7]. The sensitivity obtained here is better than the most stringent low-energy constraints for lepton-flavor violation from $\mu \to e\gamma$ [6]. We summarize our results in Sec. IV.

II. LEPTON-FLAVOR OSCILLATIONS AT $e\gamma$ COLLIDERS

The mass terms for the left-handed sleptons (partners to the left-handed leptons), right-handed sleptons and left-handed sneutrinos can be generally written as

$$\tilde{e}^*_{L\alpha} M^2_{L\alpha\beta} \tilde{e}_{L\beta} + \tilde{e}^*_{R\alpha} M^2_{R\alpha\beta} \tilde{e}_{R\beta} + \tilde{\nu}^*_{\alpha} M^2_{\tilde{\nu}\alpha\beta} \tilde{\nu}_{\beta}, \tag{1}$$

where $\alpha, \beta = 1, 2, 3$ are the generation indices, and $M_{L,R,\tilde{\nu}}$ are mass matrices which can be diagonalized through the unitary matrices $W_{L,R,\tilde{\nu}}$. In terms of the slepton mass eigenstates, the lepton-slepton interactions with gauginos are flavor non-diagonal:

$$\tilde{e}_{Li} W^*_{Lij} \overline{e}_{Lj} \tilde{\chi}^0 + \tilde{e}_{Ri} W^*_{Rij} \overline{e}_{Rj} \tilde{\chi}^0 + \tilde{\nu}_i W^*_{\tilde{\nu}ij} \overline{e}_{Lj} \tilde{\chi}^- + h.c., \tag{2}$$

which generally leads to lepton-flavor violating effects. If the slepton mass differences are large and the lepton-flavor off-diagonal couplings (W_{ij}) are sizeable, Eq. (2) may directly lead to flavor-changing processes like

$$e^-\gamma \to \tilde{\nu}_\ell \tilde{\chi}^-_i, \tag{3}$$
$$e^-\gamma \to \tilde{\ell}^- \chi^0_j, \tag{4}$$

where the flavor index $\ell = \mu, \tau$, as depicted in Fig. 1(a) and (b), in which the black dots denote the vertices with flavor changing interactions. On the other hand, if $\tilde{e}^-$ ($\tilde{\nu}_e$) is nearly degenerate with other sleptons (sneutrinos), as prefered by suppressing the FCNC and as constrained by $\mu \to e\gamma$ data, then the processes (3) and (4) may mainly go through the flavor diagonal production $\tilde{e}^- \chi^0_j (\tilde{\nu}_e \tilde{\chi}^-_i)$ followed by $\tilde{e}^- \to \tilde{\ell}^- (\tilde{\nu}_e \to \tilde{\nu}_\ell)$ oscillation subsequently [7]. The two cross sections are then related by

$$\sigma(e\gamma \to \tilde{\ell}^- \tilde{\chi}^0_1) = \sigma(e\gamma \to \tilde{e}^- \tilde{\chi}^0_1) P(\tilde{e}^- \to \tilde{\ell}^-), \tag{5}$$
$$P(\tilde{e}^- \to \tilde{\ell}^-) = 2\sin^2\theta_\ell \cos^2\theta_\ell \frac{(\triangle M^2)^2}{4\overline{m}^2\Gamma^2 + (\triangle M^2)^2},$$

where $P(\tilde{e}^- \to \tilde{\ell}^-)$ is the transition probability of interaction eigenstates $\tilde{e}^-$ to $\tilde{\ell}^-$ via oscillation, and $\triangle M^2 = m^2_{\tilde{l}} - m^2_{\tilde{e}}$, $\overline{m} = (m_{\tilde{l}} + m_{\tilde{e}})/2$, and θ_ℓ the mixing angle between $\tilde{e}^-$ and $\tilde{\ell}^-$. The cross section formula for sneutrino oscillation is the same as Eq. (5) with the replacement of $\tilde{e} \to \tilde{\nu}_e, \tilde{\ell}^- \to \tilde{\nu}_l$.

For the flavor diagonal production of $\tilde{\nu}_e \tilde{\chi}^-$, the differential cross section summed over the chargino helicity are [11]

$$\frac{d\sigma}{d\cos\theta}(e^-_-\gamma_- \to \tilde{\nu}_{eL}\tilde{\chi}^-_j) = \frac{\pi\alpha^2}{\sin^2\theta_W}\,\frac{V_{j1}^2}{s}\,\frac{r_{\tilde{\chi}}^2}{(1-\beta^2)}\frac{\beta}{(1+\beta\cos\theta)^2}$$

$$\times \sum_{\lambda=\pm1}(1+\lambda\cos\theta)(1+\lambda\beta)^2\left(\frac{\sqrt{1-\beta^2}}{r_{\tilde{\chi}}} - (1+\lambda\beta)\right), \tag{6}$$

$$\frac{d\sigma}{d\cos\theta}(e^-_-\gamma_+ \to \tilde{\nu}_{eL}\tilde{\chi}^-_j) = \frac{\pi\alpha^2}{\sin^2\theta_W}\,\frac{V_{j1}^2}{s}\,\frac{r_{\tilde{\chi}}^2}{(1-\beta^2)}\,\frac{2\beta^3\sin^2\theta(1-\beta\cos\theta)^2}{(1+\beta\cos\theta)^2}. \tag{7}$$

The subscripts on e and γ refer to the electron and photon helicities. The angle θ specifies the chargino momentum relative to the incoming direction in the c.m. frame, $\beta = p/E$ is the chargino velocity in the c.m. frame, and $r_{\tilde{\chi}} = m_{\tilde{\chi}}/\sqrt{s}$. The $(\lambda_e, \lambda_\gamma) = (-,-)$ helicity amplitude is S-wave near threshold so the cross section of Eq. (6) is proportional to β; the $(-,+)$ helicity amplitude, which comes only from the t-channel diagram, is P-wave near threshold so the cross section of Eq. (7) goes like β^3. the scattering amplitude is proportional to the wino fractions V_{j1} of the matrix V_{ji} that diagonalizes the mass matrix (the first index j labels the chargino mass eigenstate $\tilde{\chi}^+_1, \tilde{\chi}^+_2$ and the second index i refers to the primordial gaugino and Higgsino basis $\tilde{W}^\pm$, $\tilde{H}^\pm$). Further, the $\tilde{\nu}_L$ state fixes the incoming electron chirality to be left-handed "−".

Selectron-neutralino associated production $e\gamma \to \tilde{e}\tilde{\chi}^0$ proceeds via s-channel electron and t-channel selectron exchanges [9,11]; see Fig. 1(b) with $\tilde{\ell} = \tilde{e}$. By Eq. (5), we can get the cross section of $e\gamma \to \tilde{\ell}\tilde{\chi}^0$. The contributions from Higgsino components ($\tilde{H}^0_1$, $\tilde{H}^0_2$) of $\tilde{\chi}^0$ can be neglected and only the neutralino mixing elements Z_{j1} and Z_{j2} enter. After summing over the neutralino helicities, there are four independent helicity cross sections as the helicity of the $\tilde{e}_R$ ($\tilde{e}_L$) matches that of the e_R (e_L):

$$\frac{d\sigma}{d\cos\theta}(e^-_+\gamma_+ \to \tilde{e}^-_R\tilde{\chi}^0_i) = \frac{d\sigma}{d\cos\theta}(e^-_-\gamma_- \to \tilde{e}^-_L\tilde{\chi}^0_i) = \pi\alpha^2\,\frac{2F^2_{i(L,R)}}{s}\,\frac{r_{\tilde{e}}^2}{(1-\beta^2)}$$

$$\times\frac{\beta}{(1+\beta\cos\theta)^2}\,\sum_{\lambda=\pm1}(1+\lambda\cos\theta)(1+\lambda\beta)^2\left(\frac{\sqrt{1-\beta^2}}{r_{\tilde{e}}} - (1+\lambda\beta)\right), \tag{8}$$

$$\frac{d\sigma}{d\cos\theta}(e^-_+\gamma_- \to \tilde{e}^-_R\tilde{\chi}^0_i) = \frac{d\sigma}{d\cos\theta}(e^-_-\gamma_+ \to \tilde{e}^-_L\tilde{\chi}^0_i) =$$

$$\pi\alpha^2\,\frac{2F^2_{i(L,R)}}{s}\,\frac{r_{\tilde{e}}^2}{(1-\beta^2)}\,\frac{2\beta^3\sin^2\theta}{(1+\beta\cos\theta)^2}\left(\frac{\sqrt{1-\beta^2}}{r_{\tilde{e}}} - (1-\beta\cos\theta)\right). \tag{9}$$

The F_{iL} (F_{iR}) for $\tilde{e}_L$ ($\tilde{e}_R$) are effective couplings given by

$$F_{iL} = \frac{1}{2}\left[\frac{Z_{i1}}{\cos\theta_W} + \frac{Z_{i2}}{\sin\theta_W}\right], \quad F_{iR} = \frac{-Z^*_{i1}}{\cos\theta_W}. \tag{10}$$

Here the Z_{ji} are the elements of matrices that diagonalize the neutralino mass matrix (the first index j labels the neutralino mass eigenstate $\tilde{\chi}^0_j$, $j = 1...4$, and the second index $i = 1, 2$ refers to the primordial gaugino and Higgsino basis ($\tilde{B}^0$, $\tilde{W}^0$, $\tilde{H}^0_1$, $\tilde{H}^0_2$)). The angle θ specifies the direction of the selectron with respect to the direction of the incoming electron in the c.m. frame, β is the velocity of the selectron, and $r_{\tilde{e}} = m_{\tilde{e}}/\sqrt{s}$.

Due to the approximate decoupling of Higgsinos from the electron, the cross sections for the processes (3) and (4) are only large when the charginos and neutralinos are mainly gaugino-like, namely $\tilde{\chi}^{\pm} \sim \tilde{W}^{\pm}$ and $\tilde{\chi}^0_1 \sim \tilde{B}^0$, $\tilde{\chi}^0_2 \sim \tilde{W}^0$. Fortunately gaugino-like $\tilde{\chi}^{\pm}_1$, $\tilde{\chi}^0_1$ and $\tilde{\chi}^0_2$ are highly favored theoretically for two reasons: (*i*) the radiative electroweak symmetry breaking in SUSY GUTs theories yields a large $|\mu|$ value if $\tan\beta$ is bounded by the infrared fixed point solutions for the top quark Yukawa coupling [14,15]; (*ii*) $\chi^0_1 \sim \tilde{B}$ is strongly preferred for χ^0_1 to be a viable cold dark matter candidate [14–16]. In the rest of our paper, we will thus concentrate on this scenario. For our illustrations we choose the chargino/neutralino masses (in GeV)

$$m_{\tilde{\chi}^0_1} = 64, \qquad m_{\tilde{\chi}^0_2} = 130, \qquad m_{\tilde{\chi}^{\pm}_1} = 130, \qquad m_{\tilde{\chi}^{\pm}_2} = 294, \tag{11}$$

and the mixing matrix elements

$$Z_{11} = 0.95, \qquad Z_{12} = -0.20, \qquad Z_{21} = -0.28, \qquad Z_{22} = -0.90, \tag{12}$$

for the neutralinos and

$$V_{11} = 0.96, \qquad V_{21} = -0.27, \tag{13}$$

for the chargino. These parameters correspond to the following MSSM parameters at the weak scale

$$M_1 = 62 \text{ GeV}, \quad M_2 = 126 \text{ GeV}, \quad \mu = 265 \text{ GeV} \ , \quad \tan\beta = 3 \ , \tag{14}$$

where $\tan\beta$ is a little larger than that at the infrared fixed point value [14] to get a heavier Higgs mass to avoid the LEP2 limit and the convention for sign(μ) follows Ref. [14]. For slepton masses, we choose (in GeV)

$$m_{\tilde{\mu}_L} \approx m_{\tilde{e}_L} = 275, \qquad m_{\tilde{\mu}_R} \approx m_{\tilde{e}_R} = 260, \qquad m_{\tilde{\nu}_\mu} \approx m_{\tilde{\nu}_e} = 266. \tag{15}$$

Our choices for the gaugino and slepton masses are consistent with renormalization group evolution [15] to the electroweak scale, with the following universal mSUGRA parameters

$$m_0 = 250 \text{ GeV}\,, \qquad m_{1/2} = 150 \text{ GeV}\,, \qquad A = 0\,. \tag{16}$$

From Eqs. (6–9), we see the following features: Due to the stronger diagonal couplings Z_{ii}, the cross sections for $\tilde{e}_L\tilde{\chi}^0_2$ (mainly $\tilde{e}_L\tilde{W}^0$) and $\tilde{e}_R\tilde{\chi}^0_1$ (mainly $\tilde{e}_R\tilde{B}^0$) are significantly larger than the other selectron channels; the weaker neutral current couplings and the more massive scalar propagator in selectron production make their cross sections smaller than those for sneutrino production. We illustrate these features in four processes with larger cross sections in Fig. 2. Two non-zero e, γ helicity combinations are labeled in parentheses. The solid curves are of S-wave near the threshold resulting in a higher cross section rate, and the dashed ones of P-wave. This indicates the possible signal enrichment by properly choosing the helicity configuration for the beams. The lower curves show the effects of convolution with the backscattered laser photon spectrum for the machine parameters as chosen in Refs. [10,11]. The effect is to decrease the cross sections by about a factor of two. At an NLC with c. m. energy 500 GeV, the typical production sections are of order 1000 fb for $e\gamma \to \tilde{\nu}_e\tilde{\chi}^-_1$, and about 100 fb for $e\gamma \to \tilde{e}_L\tilde{\chi}^0_2$, and $\tilde{e}_R\tilde{\chi}^0_1$, on which three channels we will focus for our phenomenology study in the next section.

TABLE I. Sparticle decay modes and branching fractions for the representative parameter choice. Here q generically denotes a quark and l denotes a lepton; fermion-antifermion pairs $f\bar{f}'$ with net charge $-1(0)$ are denoted by $C^-(N^0)$

Decay Modes	Branching Fraction (%)
$\tilde{\chi}_1^- \to \tilde{\chi}_1^0 C^-$	79.5 ($\tilde{\chi}_1^0 q\bar{q}'$), 20.5 ($\tilde{\chi}_1^0 l^- \nu$)
$\tilde{\chi}_2^0 \to \tilde{\chi}_1^0 N^0$	72 ($\tilde{\chi}_1^0 q\bar{q}$), 19 ($\tilde{\chi}_1^0 \nu\bar{\nu}$), 9 ($\tilde{\chi}_1^0 l^+ l^-$)
$\tilde{\mu}_R \to \tilde{\chi}_1^0 \mu^-$	100
$\tilde{\mu}_L \to \tilde{\chi}_1^- \nu,\ \tilde{\chi}_2^0 \mu^-,\ \tilde{\chi}_1^0 \mu^-$	54, 28, 18
$\tilde{\nu}_\mu \to \tilde{\chi}_1^+ \mu^-,\ \tilde{\chi}_2^0 \nu,\ \tilde{\chi}_1^0 \nu$	61, 29, 10

III. SIGNAL SELECTION AND BACKGROUND SUPPRESSION

We first consider the $e-\mu$ flavor oscillation. The muon slepton and sneutrino production rates can be obtained by Eqs. (5–9). Before considering the experimental signature at an $e\gamma$ collider, in Table I we illustrate the predicted branching fractions of the final state sparticle decays [17] for the parameters discussed earlier. We have introduced notations $C^\pm, N^0$ to denote the net charge of the final $f\bar{f}'$. They are largely from $W^{*\pm}, Z^{*0}$ decays, so that we can more directly compare with SM background processes. The decay widths for the sleptons are also an important variable in the calculation of Eq. (5). They are calculated to be $\Gamma_{\tilde{\ell}_R} = 1.2$ GeV, $\Gamma_{\tilde{\ell}_L} = 2.6$ GeV and $\Gamma_{\tilde{\nu}_L} = 2.1$ GeV for the parameters discussed in the last section. The neutrinos and χ_1^0 result in missing energies in the detector; while the light quarks will lead to hadronic jets. Combining the sparticle production and decay, we classify the final state signatures in Table II with corresponding branching fractions. The decays of the sparticles in these reactions generally give distinctive signals: Large missing energy ($\not{E}$), energetic charged leptons or jets from light quarks. To effectively suppress the SM background, we utilize the following channels:

$$e^-\gamma \to \tilde{\nu}_\mu \tilde{\chi}_1^- \to \mu^- \not{E}\ q\bar{q}'\ q\bar{q}', \tag{17}$$

to probe the mixing angle $\theta_{\nu L}$ between $\tilde{\nu}_e$ and $\tilde{\nu}_\mu$; the process

$$e^-\gamma \to \tilde{\mu}_L \tilde{\chi}_2^0 \to \mu^- \not{E}\ q\bar{q}\ q\bar{q}, \tag{18}$$

for θ_L between $\tilde{e}_L$ and $\tilde{\mu}_L$ and the process

$$e^-\gamma \to \tilde{\mu}_R \tilde{\chi}_1^0 \to \mu^- \not{E}, \tag{19}$$

for θ_R between $\tilde{e}_R$ and $\tilde{\mu}_R$.

Generally speaking, due to the distinctive kinematical characteristics, the multiple-jet ($q\bar{q}'$) signals for $\tilde{\nu}_\mu \tilde{\chi}_1^-$ and $\tilde{\mu}_L \chi_2^0$ have favorable signal-to-background ratios. The irreducible SM background processes are

$$e^-\gamma \to \mu^- \nu_\mu\ W^- W^+, \quad \mu^- \nu_\mu\ ZZ. \tag{20}$$

TABLE II. Sparticle production and decay in $e^-\gamma$ collisions. Branching fractions based on Table I are given in the parentheses. Here $\not{E}$ denotes missing energy resulting from $\tilde{\chi}_1^0$ and ν final state; C^- (N^0) denotes a fermion-antifermion pair of charge -1 (0).

Process	Final State & Branching Fraction
$e^-\gamma \to \tilde{\nu}_\mu \chi_1^- \to$	$C^- \not{E}$ (16%), $C^- N^0 \not{E}$ (23%), $C^- C^+ \mu^- \not{E}$ (61%)
$e^-\gamma \to \tilde{\mu}_L \tilde{\chi}_2^0 \to$	$N^0 \mu^- \not{E}$ (23%), $N^0 N^0 \mu^- \not{E}$ (18%), $C^- N^0 \not{E}$ (44%), $C^- \not{E}$ (15%)
$e^-\gamma \to \tilde{\mu}_R \tilde{\chi}_1^0 \to$	$\mu^- \not{E}$ (100%)

Including the hadronic decay branching fractions of W, Z decays, we find that the cross sections of Eq. (20) are less than 0.1 fb at $\sqrt{s}_{ee} = 500$ GeV. We could therefore expect a very effective probe to the oscillation parameters for processes (17) and (18). However, the leading background to the $\tilde{\mu}_R \tilde{\chi}_1^0$ signal of Eq. (19) is

$$e^-\gamma \to \mu^- \bar{\nu}_\mu \nu_e. \tag{21}$$

The total cross section for this process at $\sqrt{s}_{ee} = 500$ GeV is about two picobarns, and the oscillation signal would be swamped by it. On the other hand, this signal process involves a right-handed electron in the initial state while the background process involves only a left-handed one due to the W exchange. If high beam polarization e_R^- can be implemented [12], then this SM background can be highly suppressed. Helicity argument shows that choosing the right-handed photon beam could also help further suppress the background survived from the impure $e_L^- \gamma_+$ reaction, without hurting the signal [see Fig. 2(b)]. We thus assume that the background Eq. (21) can been reduced to a manageable level. In our subsequent numerical discussions, based on the signal branching ratios in Table II, we estimate the signal efficiencies to be 40%, 15% and 80% for Eqs. (17), (18) and (19), respectively. We consider an oscillation signal to be observable if the cross section after the inclusion of the efficiencies to be no less than 0.1 fb. For instance, a 0.1 fb signal cross section and negligible backgrounds with a 50 fb^{-1} luminosity would correspond to about 99% C.L. discovery.

In Figs. 3, 4 and 5, we illustrate contours of constant cross sections for signal processes in (17), (18) and (19), respectively, in $\triangle M^2 - \sin 2\theta_\ell$ plane. When plotting each figure, we assume that just one mixing angle exits, *i.e.*, the contributions originating from other mixing angles are set to zero. The (thick) solid curves in the figures present the constant cross section contours for $\sigma = 0.1$, 0.5 and 1 fb. The dashed lines correspond to the current bound on the branching fraction $B(\mu \to e\gamma) < 4.9 \times 10^{-11}$. A lower value of 4.9×10^{-12} is also indicated by the (thin) solid line. Those curves are obtained with the SUSY parameters presented in the previous section. As showed in Figs. 3 and 4, achievable sensitivity in $\triangle M^2 - \sin 2\theta_\ell$ for the left-handed slepton sector can be significantly better than the low-energy constraint from $\mu \to e\gamma$. It is even more impressive to probe the oscillation parameters in the right-handed slepton sector if the beam polarizations can be implemented to suppress the backgrounds. Compared with the resultes at e^+e^- and e^-e^- colliders [7], the potential of probing mixing angle θ_R between $\tilde{\mu}_R$ and $\tilde{e}_R$ are comparable.

So far, we have only discussed the slepton oscillations between electron and muon flavors. Our analyses are essentially applicable for $\tilde{e} - \tilde{\tau}$ oscillation as well. In fact, our calculations for the signal by Eqs. (5)–(9) and the backgrounds of Eqs. (20)-(21) should be formally identical for the τ final state. The only differences are: Theoretically, the mass difference between $\tilde{e}$ and $\tilde{\tau}$ may be bigger than that of $\tilde{e}$ and $\tilde{\mu}$ due to the larger Yukawa coupling running for $\tilde{\tau}$. Experimentally, the τ lepton tagging is less efficient than that for μ. This may lead to about a 80% reduction on the event rate. Nevertheless, we expect about same order of magnitude sensitivity for $\tilde{e}-\tilde{\tau}$ oscillation. Due to the electron flavor in the initial state, the signal processes under discussion are not sensitive to the $\tilde{\mu}-\tilde{\tau}$ oscillation. Recent study [18] showed that an e^+e^- collider could probe this oscillation to high precision.

IV. DISCUSSIONS AND SUMMARY

We only considered a representative set of SUSY parameters. As long as the lighter neutralino and chargino are gaugino-like as anticipated in mSUGRA models and in the minimal gauge-mediated SUSY breaking model, our results should be generally valid. We presented our study with the slepton masses approximately 270 GeV. This has been beyond the reach for an NLC with $\sqrt{s_{ee}}=500$ GeV via $e^+e^- \to \tilde{\ell}^-\tilde{\ell}^+, \tilde{\nu}\tilde{\nu}^*$. For a heavier slepton spectrum, we would need a collider with a higher c. m. energy. The current discussions on the linear collider parameters [12] indicate the feasibility to extend the c. m. energy to 1.5 TeV. It is always most beneficial that the c. m. energy is just above the signal production threshold. However, if the neutralino and chargino are Higgsino-like, then their couplings to leptons are too weak to result in significant cross sections for the signal at an $e\gamma$ collider.

In summary, we have demonstrated that for gaugino-like neutralino and chargino, the slepton oscillation effects may be observable at a 500 GeV $e\gamma$ collider with a 50 fb^{-1} luminosity. The achievable sensitivity in $\triangle M^2 - \sin 2\theta_\ell$ for the left-handed slepton sector can be significantly better than the low-energy constraint from $\mu \to e\gamma$. In the right-handed slepton sector, our results are comparable to that for e^+e^- and e^-e^- colliders, if the beam polarizations (e^-_R and γ_+) can be implemented to suppress the backgrounds. It may even be possible for an $e\gamma$ collider to go beyond the probe at an e^+e^- collider because of the kinematics advantage. Our analyses are essentially applicable for $\tilde{e}-\tilde{\tau}$ oscillation, with a sensitivity of the same order of magnitude as that for $\tilde{e}-\tilde{\mu}$.

ACKNOWLEDGMENTS

We thank H.-C. Cheng and J. Feng for discussions. This work was supported in part by the U. S. Department of Energy under Grant No. DE-FG02-95ER40896 and by National Natural Science Foundation of China. Further support was provided by the University of Wisconsin Research Committee, with funds granted by the Wisconsin Alumni Research Foundation.

REFERENCES

[1] For recent reviews on SUSY collider phenomenology, see *e. g.*, X. Tata, UH-511-872-97 [hep-ph/9706307]; V. Barger, MADPH-97-1011 [hep-ph/9801440]; J. F. Gunion and H. E. Haber, SCIPP-97-37 [hep-ph/9806330], to appear in *Perspectives on Supersymmetry*, G. L. Kane, ed. (World Scientific, 1998).

[2] J. S. Hagelin, S. Kelley and T. Tanaka, Nucl. Phys. **B415**, 293 (1994); E. Gabrielli, A. Masiero and L. Silvestrini, Phys. Lett. **B374**, 80 (1996).

[3] Super-Kamiokande collaboration, BU-98-17 [hep-ex/9807003].

[4] S. Bertolini, F. Borzumati, A. Masiero and G. Ridolfi, Nucl. Phys. **B353**, 591 (1991); J. Wu, R. Arnowitt and P. Nath, Phys. Rev. **D51**, 1371 (1995); V. Barger, M. Berger, P. Ohmann and R. Phillips, Phys. Rev. **D51**, 2438 (1995); H. Baer, M. Brhlik, D. Castano, X. Tata, Phys. Rev. **D58**, 015007 (1998).

[5] F. Gabbiani, E. Gabrielli, A. Masiero and L. Silvestrini, Nucl. Phys. **B477**, 321 (1996).

[6] F. Borzumati and A. Masiero, Phys. Rev. Lett. **57**, 44 (1986); F. Gabbiani and A. Masiero, Nucl. Phys. **B322**, 235 (1989); R. Barbieri, L. Hall, A. Strumia, Nucl. Phys. **B445**, 219 (1995); David W. Sutter, hep-ph/9704390.

[7] N. Arkani-Hamed, H.-C. Cheng, J. L. Feng, L. J. Hall, Phys. Rev. Lett. **77**, 1937 (1996).

[8] N. Arkani-Hamed, H.-C. Cheng, J. L. Feng, L. J. Hall, Nucl. Phys. **B505**, 3 (1997).

[9] F. Cuypers, G.J. van Oldenberg, and R. Rückl, Nucl. Phys. **B383**, 45 (1992); H.A. König and K.A. Peterson, Phys. Lett. **B294**, 110 (1992); D.L. Borden, D. Bauer and D.O. Caldwell, SLAC preprint SLAC-PUB-5715 (1992); T. Kon and A. Goto, Phys. Lett. **B295**, 324 (1992); D. Choudhury and F. Cuypers, Nucl. Phys. **B451**, 16 (1995); K. Kiers, J.N. Ng and G.H. Wu, Phys. Lett. **B381**, 177 (1996).

[10] T. Kon and A. Goto, Phys. Lett. **B451**, 16 (1995).

[11] V. Barger, T. Han and J. Kelly, Phys. Lett. **B419**, 233 (1998).

[12] Report submitted to Snowmass 96, *Physics and Technology of the Next Linear Collider*, BNL 52-502 (1996).

[13] H.F. Ginzburg, G.L. Kotkin, V.G. Serbo and V.I. Telnov, Nucl. Inst. and Meth. **205**, 47 (1983); H.F. Ginzburg, G.L. Kotkin, S.L. Panfil, V.G. Serbo and V.I. Telnov, Nucl. Inst. and Meth. **219**, 5 (1984).

[14] V. Barger, M. S. Berger and P. Ohmann, Phys. Rev. **D 47**, 1093 (1993); Phys. Rev. **D49**, 4908 (1994); V. Barger, M. S. Berger, P. Ohmann and R. J. N. Phillips, Phys. Lett. **B314**, 351(1993); P. Langacker and N. Polonsky, Phys. Rev. **D50**, 2199 (1994); W. A. Bardeen, M. Carena, S. Pokorski and C. E. M. Wagner, Phys. Lett. **B320**, 110(1994); B. Schremp, Phys. Lett. **B344**, 193(1995).

[15] Analyses of supergravity mass patterns include: G. Ross and R. G. Roberts, Nucl. Phys. **B377**, 571 (1992); R. Arnowitt and P. Nath, Phys. Rev. Lett. **69**, 725 (1992); M. Drees and M. M. Nojiri, Nucl. Phys. **B369**, 54 (1993); S. Kelley, J. Lopez, D. Nanopoulos, H. Pois and K. Yuan, Nucl. Phys. **B398**, 3 (1993); M. Olechowski and S. Pokorski, Nucl. Phys. **B404**, 590(1993); V. Barger, M. Berger and P. Ohmann, Phys. Rev. **D49**, 4908(1994).

[16] See *e.g.*, K. A. Olive and M. Srednicki, Nucl. Phys. **B355**, 208 (1991); M. Drees and M. Nojiri, Phys. Rev. **D47**, 376(1993); R. G. Roberts and L. Roszkowski, Phys. Lett. **B309**, 329(1993).

[17] H. Baer, F. Paige, S. Protpopescu and X. Tata, in *Proceedings of the Workshop On*

Physics at Current Accelerators and Supercolliders, eds. J. Hewitt, A. White and D. Zeppenfeld, Argonne National Laboratory (1993).

[18] J. Hisano, M. Nojiri, Y. Shimizu and M. Tanaka, KEK-TH-586 [hep-ph/9808410].

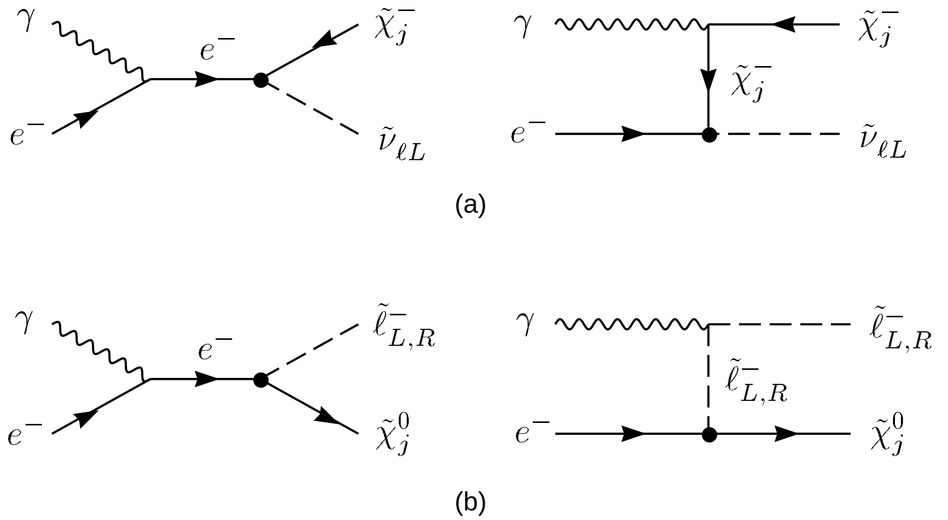

FIG. 1. Feynman graphs for slepton-gaugino associated production (a) $e^-\gamma \to \tilde{\nu}_\ell \tilde{\chi}^-$ and (b) $e^-\gamma \to \tilde{l}^- \tilde{\chi}^0$. The black dots denote the new flavor violating vertices.

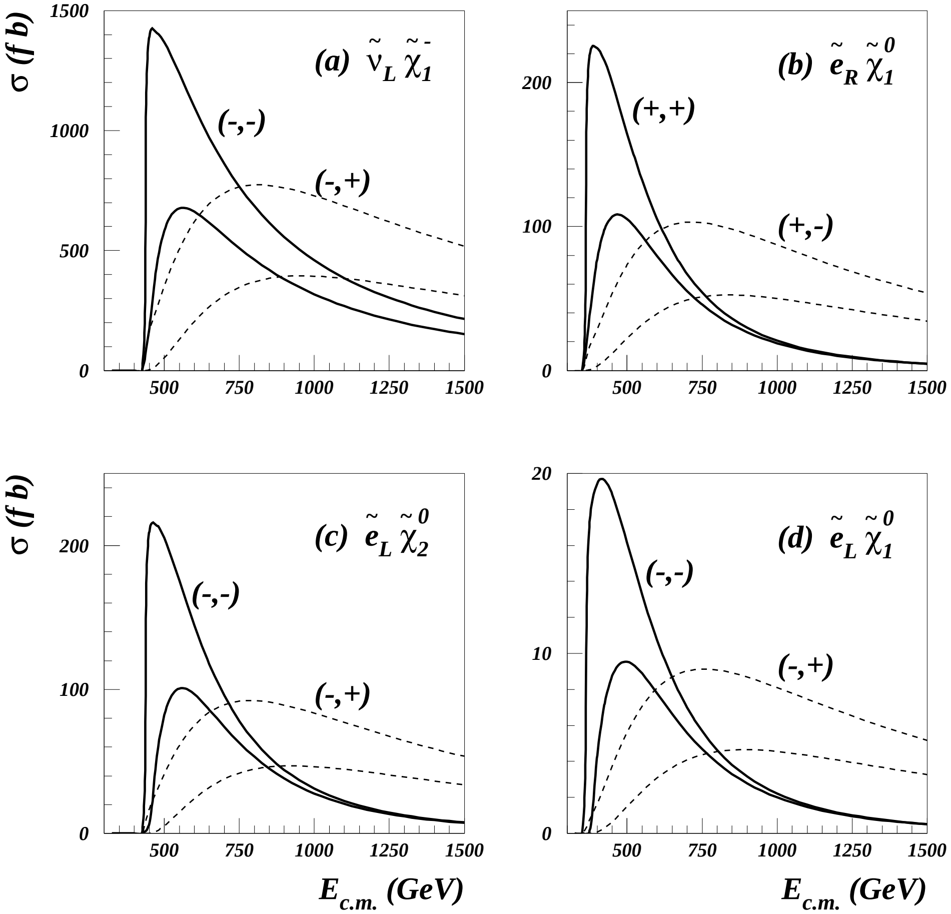

FIG. 2. Total cross section in fb versus the c. m. energy in GeV for (a) $e\gamma \to \tilde{\nu}_e \tilde{\chi}_1^-$, (b) $e\gamma \to \tilde{e}_R \tilde{\chi}_1^0$, (c) $e\gamma \to \tilde{e}_L \tilde{\chi}_1^0$ and (d) $e\gamma \to \tilde{e}_L \tilde{\chi}_2^0$, with the SUSY parameters given in the text. Electron and photon beam polarizations are indicated in the parentheses. The upper two curves are these at $e\gamma$ collider versus $\sqrt{s_{e\gamma}}$. The lower two curves are the corresponding results, convoluted with the backscattered photon spectrum, versus $\sqrt{s_{ee}}$.

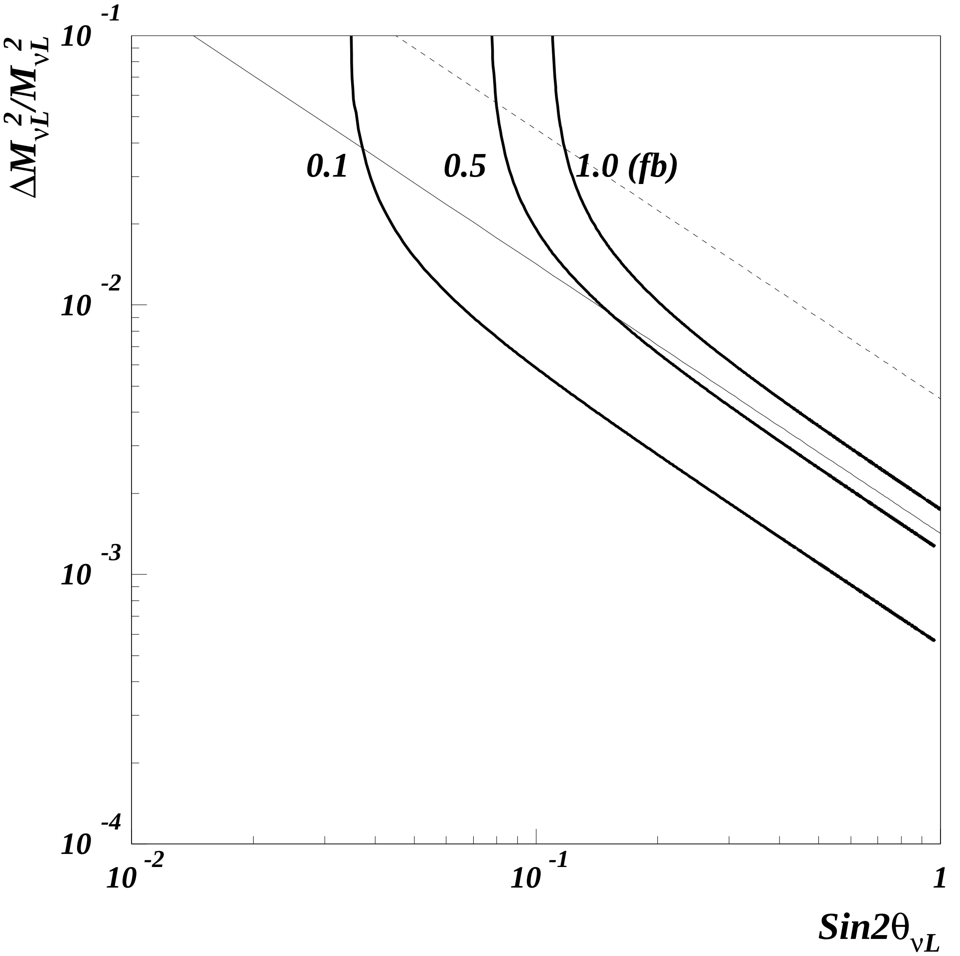

FIG. 3. Contours of constant cross sections for $e^-\gamma \rightarrow \tilde{\nu}_\mu\tilde{\chi}_1^- \rightarrow \mu^-\ \not{E}\ q\bar{q}'\ q\bar{q}'$ (thick solid) with $\sqrt{s_{ee}} = 500$ GeV and the SUSY parameters given in the text. Constant contours of $B(\mu \rightarrow e\gamma) = 4.9 \times 10^{-11}$ (dotted) and 4.9×10^{-12} (solid) are also plotted.

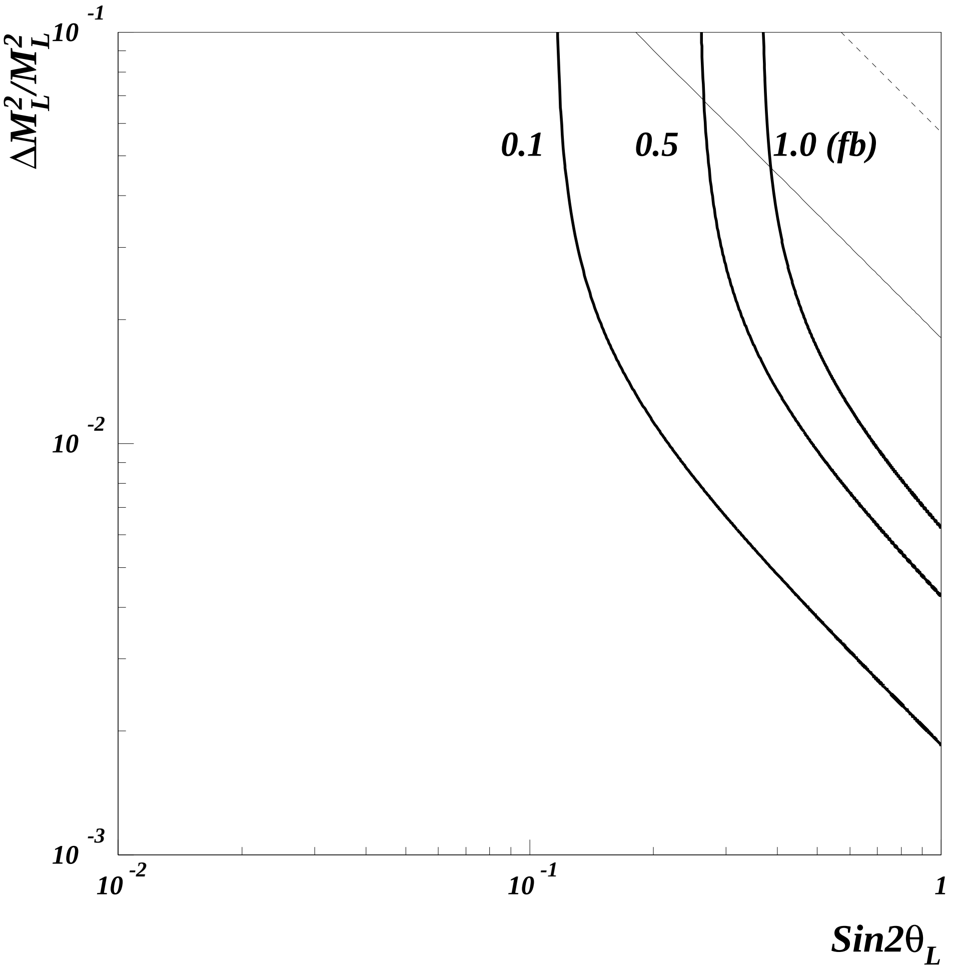

FIG. 4. Contours of constant cross sections for $e^-\gamma \rightarrow \tilde{\mu}_L\tilde{\chi}_2^0 \rightarrow \mu^- \not{E}\ q\bar{q}\ q\bar{q}$ (thick solid) with $\sqrt{s_{ee}} = 500$ GeV and the SUSY parameters given in the text. Constant contours of $B(\mu \rightarrow e\gamma) = 4.9 \times 10^{-11}$ (dotted) and 4.9×10^{-12} (solid) are also plotted.

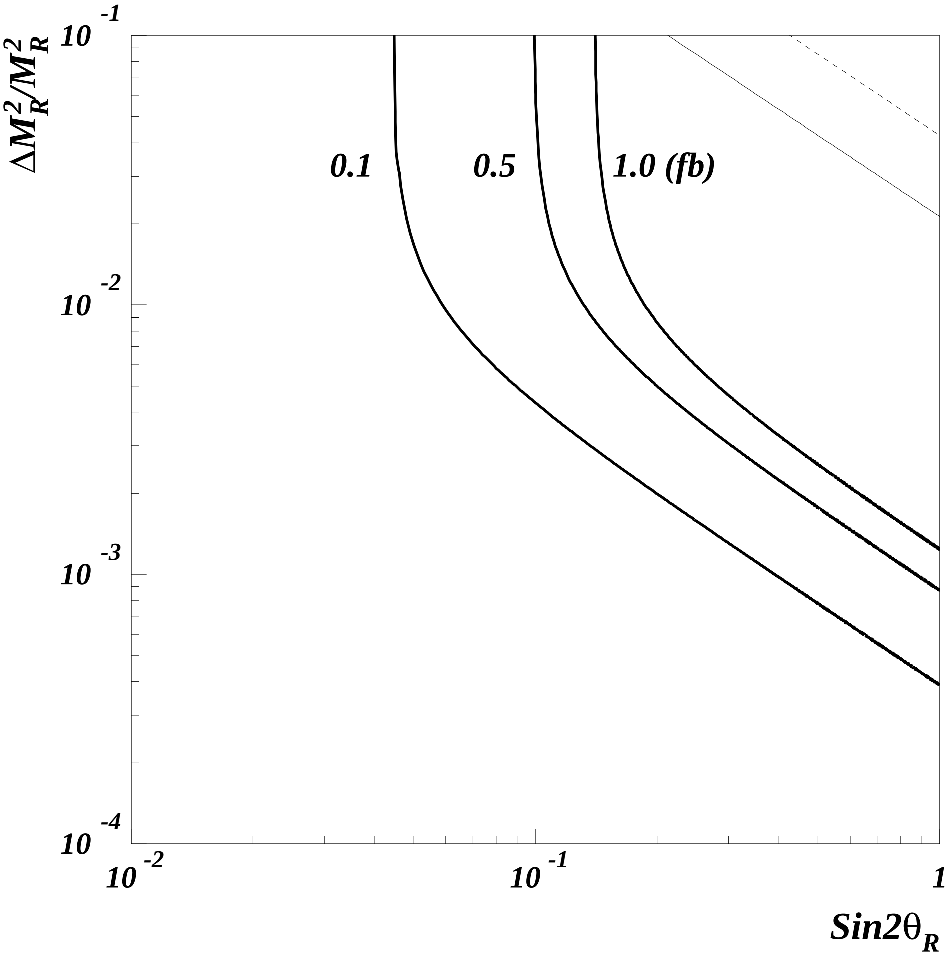

FIG. 5. Contours of constant cross sections for $e_R^- \gamma_+ \rightarrow \tilde{\mu}_R \tilde{\chi}_1^0 \rightarrow \mu^- \not{E}$ (thick solid) with $\sqrt{s_{ee}} = 500$ GeV and the SUSY parameters given in the text. Constant contours of $B(\mu \rightarrow e\gamma) = 4.9 \times 10^{-11}$ (dotted) and 4.9×10^{-12} (solid) are also plotted.